International Journal of Engineering Inventions
e-ISSN: 2278-7461, p-ISSN: 2319-6491
Volume 15, Issue 6 [June 2026] PP: 225-236

Comparative Performance and Robustness Analysis of NARMA-L2 Neural and PID Controllers for Frequency Regulation in an Interconnected Two-Area Hydropower System under Load Disturbances and Parametric Uncertainty

Duy-Trung Nguyen[1,*], Van-Hoat Hoang[2], Tran Thi Kim Thanh[3]
Hoai-Son Nguyen[4]
[1]*Faculty of Control and Automation, Electric Power University, Hanoi, Vietnam*
[2]*TTH Vietnam Automation Company, LTD, Hanoi, Vietnam*
[3]*Practice and Experiment Center, Electric Power University, Hanoi, Vietnam*
[4]*Faculty of Electrical Engineering, Electric Power University, Hanoi, Vietnam*
[*]*Corresponding Author*

ABSTRACT: *This study compares a nonlinear autoregressive moving-average L2 (NARMA-L2) neural controller with a conventional proportional–integral–derivative (PID) controller for frequency regulation in an interconnected two-area hydropower system. The dynamic model incorporates hydraulic-turbine non-minimum-phase behavior, permanent and transient droop, governor–servomotor dynamics, generator–load inertia, frequency-dependent loads, tie-line power exchange, gate-position saturation, and gate-rate constraints. The NARMA-L2 model is identified using excitation data generated from plants with key parameters varied within ±25%. Its nonlinear affine functions are estimated by a shallow neural network trained through an extreme-learning formulation, while a damped inverse law determines the supplementary control input. Controller performance is evaluated under step and band-limited random load disturbances for both nominal and perturbed plants. Robustness is further examined using twelve Monte Carlo parameter realizations. For step-load disturbances, NARMA-L2 reduces the total frequency integral absolute error from 0.1799 to 0.1292 Hz·s for the nominal plant and from 0.1924 to 0.1295 Hz·s for the perturbed plant. Under random loading, the corresponding reductions are from 0.4336 to 0.2543 Hz·s and from 0.4591 to 0.3020 Hz·s, respectively. The neural controller also achieves lower peak and root-mean-square frequency deviations across the investigated cases. This improvement is obtained at the cost of greater control activity and, in some step-load conditions, a larger transient tie-line power deviation. Overall, NARMA-L2 provides superior disturbance attenuation and resilience to parameter variations, whereas PID offers lower implementation complexity and more moderate actuator utilization.*

Keywords: *automatic generation control; hydropower governor; load-frequency control; NARMA-L2; neural control; PID control; random load; robustness; two-area power system.*

NOMENCLATURE

Symbol	Description	Unit
Δf_i	Frequency/speed deviation in area i	Hz
ΔP_{Li}	Incremental load disturbance in area i	pu
ΔP_{mi}	Incremental mechanical power	pu
ΔP_{tie}	Incremental tie-line power from area 1 to area 2	pu
H_i	Equivalent inertia constant	s
D_i	Load-damping coefficient	pu/Hz
R_i	Permanent speed droop	Hz/pu
R_{ti}	Temporary droop coefficient	Hz/pu
T_{gi}	Governor/servomotor time constant	s
T_{wi}	Water starting time	s
T_{ri}	Transient-droop reset time	s
T_{12}	Synchronizing coefficient	pu/Hz

Symbol	Description	Unit
B_i	Frequency-bias coefficient	pu/Hz
ACE_i	Area control error	pu
u_i	Secondary governor command	pu
$F(\cdot), G(\cdot)$	NARMA-L2 affine nonlinear mappings	-
d	NARMA-L2 prediction delay	samples
K_p, K_i, K_d	PID gains	-
IAE	Integral of absolute frequency error	Hz·s
ITAE	Integral of time-weighted absolute frequency error	Hz·s²

Date of Submission: 13-06-2026 Date of acceptance: 27-06-2026

I. INTRODUCTION

Frequency regulation remains a central operational requirement in interconnected power systems because active-power imbalance immediately appears as rotor-speed and frequency deviation. The problem becomes more demanding in hydropower-dominated areas. Water-column inertia creates an initial inverse mechanical-power response, turbine-governor parameters change with operating head and gate position, and tie-line coupling transfers a local disturbance to neighboring areas. Contemporary reviews therefore treat load-frequency control as a multi-time-scale and uncertainty-sensitive problem rather than a simple integral-control task [1]-[5].

Hydropower is particularly valuable for frequency support because its units can change power rapidly and can sustain regulation for periods much longer than inverter-based storage. Nevertheless, a fast gate command does not directly imply a fast positive power response. The classical hydraulic-turbine transfer function contains a right-half-plane zero; opening the gate initially reduces the turbine pressure and may briefly decrease mechanical power. Detailed modeling, validation, and dynamic-response studies consequently emphasize the water starting time, transient droop, servomotor limits, and operating-point dependence [6]-[10]. These effects can weaken a controller that was tuned on a simplified first-order turbine.

PID control is still widely used in power-plant governors and secondary frequency loops. Its structure is transparent, computationally inexpensive, and compatible with industrial implementation. Many studies have improved PID performance by optimization, fuzzy scheduling, fractional calculus, linear-matrix-inequality design, and explicit margin constraints [11]-[17]. Fixed gains, however, must represent a compromise. A tuning that is satisfactory for one loading pattern may become slow, oscillatory, or unnecessarily aggressive when inertia, water starting time, droop, and tie-line stiffness drift simultaneously.

Neural control offers a different route. A NARMA-L2 controller identifies the forward nonlinear dynamics and algebraically inverts an approximate affine input-output model. The method is a feedback-linearization strategy, not merely a black-box replacement for PID. It has been applied to multi-area frequency control, microgrids, electromechanical drives, and nonlinear converters [18]-[22]. Yet the published hydropower comparisons often use only one step disturbance, neglect the non-minimum-phase hydraulic response, or assess the neural controller on the same nominal plant used for identification. Random loading and structured parameter uncertainty are less frequently examined together.

This paper addresses that gap through a controlled, reproducible benchmark. Its main contributions are threefold. First, a two-area hydro-hydro model is developed with transient droop compensation, hydraulic non-minimum-phase dynamics, gate saturation, gate-rate limitation, generator-load dynamics, and tie-line exchange. Second, a multi-input augmented NARMA-L2 controller is trained over a ±25% parameter family and compared with a fixed PID controller using the same actuator constraints and sampling period. Third, performance is evaluated for step and random loads on nominal, representative perturbed, and Monte-Carlo plants. The comparison includes peak deviation, root-mean-square error, IAE, ITAE, tie-line excursion, and control effort, so the advantages and costs of neural inversion are both visible.

II. OVERVIEW OF SPEED REGULATION

A. Hierarchical role of hydropower speed control

A hydropower unit normally participates in primary and secondary frequency regulation. The primary governor reacts locally to speed deviation through permanent droop, thereby arresting the frequency decline and

sharing the disturbance among generating units. Temporary droop and reset compensation are added because a pure high-gain governor can destabilize the inverse hydraulic response. Secondary control acts more slowly on the speed-changer reference. In an interconnected system, this loop is driven by the area control error and is expected to restore both frequency and scheduled tie-line exchange [1], [6], [23].

For area i, the area control error is

$$ACE_1(k) = B_1\Delta f_1(k) + \Delta P_{tie}(k), \quad (1a)$$

$$ACE_2(k) = B_2\Delta f_2(k) - \Delta P_{tie}(k). \quad (1b)$$

The bias coefficient is selected as $B_i = D_i + 1/R_i$ in the nominal design. A negative frequency deviation after a load increase therefore creates a secondary command that raises the gate reference. Because the hydro turbine responds inversely at first, the controller must avoid large and rapid alternating commands.

B. Control approaches and remaining issue

Classical AGC research has produced PI/PID, optimal, robust, sliding-mode, fuzzy, and model-predictive solutions [11]-[17], [24]-[31]. Intelligent optimization can tune fixed gains efficiently, but the resulting controller still represents one point in a wide parameter space. Robust and sliding-mode designs improve uncertainty rejection, although their implementation can require state observers, gain bounds, and chattering mitigation. Data-driven and neural methods can represent nonlinear dynamics directly, but their training coverage and inverse-model conditioning must be stated explicitly [18]-[22], [32]-[35].

The present comparison therefore keeps the plant, sampling, saturation, and disturbance scenarios identical. The PID gains are fixed after nominal tuning. The NARMA-L2 model is trained offline using excitation trajectories generated from plants sampled within the specified uncertainty box. No controller is retuned during the four principal tests.

III. MATHEMATICAL MODEL OF THE TWO-AREA HYDROPOWER PLANT

A. Hydro governor and transient-droop compensation

Let u_i denote the secondary governor command and $v_i = u_i - \Delta f_i/R_i$ the combined speed-changer and permanent-droop signal. The transient-droop compensator is represented by

$$G_{ri}(s) = \frac{1 + T_{ri}s}{1 + a_i T_{ri}s}, \qquad a_i = \frac{R_{ti}}{R_i}. \quad (2)$$

Introducing the compensator state z_i gives

$$\dot{z}_i = \frac{-z_i + v_i}{a_i T_{ri}}, \qquad w_i = \frac{1}{a_i}v_i + \left(1 - \frac{1}{a_i}\right)z_i. \quad (3)$$

The gate-servomotor dynamics are

$$\dot{g}_i = \mathrm{sat}_{\dot{g}_{\min}}^{\dot{g}_{\max}}\left(\frac{-g_i + w_i}{T_{gi}}\right), \qquad |g_i| \le g_{\max}. \quad (4)$$

In this study, $g_{\max} = 0.35$ pu and $|\dot{g}_i| \le 0.15$ pu/s. These nonlinear limits are applied to both controllers.

B. Hydraulic turbine

The linearized non-elastic water-column model is

$$G_{ti}(s) = \frac{\Delta P_{mi}(s)}{g_i(s)} = \frac{1 - T_{wi}s}{1 + 0.5T_{wi}s}. \quad (5)$$

A convenient state realization uses the water-flow state q_i:

$$\dot{q}_i = \frac{-q_i + g_i}{0.5T_{wi}}, \qquad \Delta P_{mi} = 3q_i - 2g_i. \quad (6)$$

Equation (6) preserves the unit steady-state gain and the inverse initial response of (5).

C. Generator-load and tie-line equations

The incremental swing equations are

$$2H_1\Delta\dot{f}_1 = \Delta P_{m1} - \Delta P_{L1} - D_1\Delta f_1 - \Delta P_{tie}, \quad (7a)$$

$$2H_2\Delta\dot{f}_2 = \Delta P_{m2} - \Delta P_{L2} - D_2\Delta f_2 + \Delta P_{tie}. \quad (7b)$$

The tie-line power deviation follows

$$\Delta\dot{P}_{tie} = 2\pi T_{12}(\Delta f_1 - \Delta f_2). \quad (8)$$

The complete state vector is

$$\mathbf{x} = [\Delta f_1 \quad z_1 \quad g_1 \quad q_1 \quad \Delta f_2 \quad z_2 \quad g_2 \quad q_2 \quad \Delta P_{tie}]^T. \quad (9)$$

The nonlinear model is integrated by a fourth-order Runge-Kutta scheme with a 0.1 s sampling interval. Figure 1 shows the two-area structure and the common feedback signals used by the controllers.

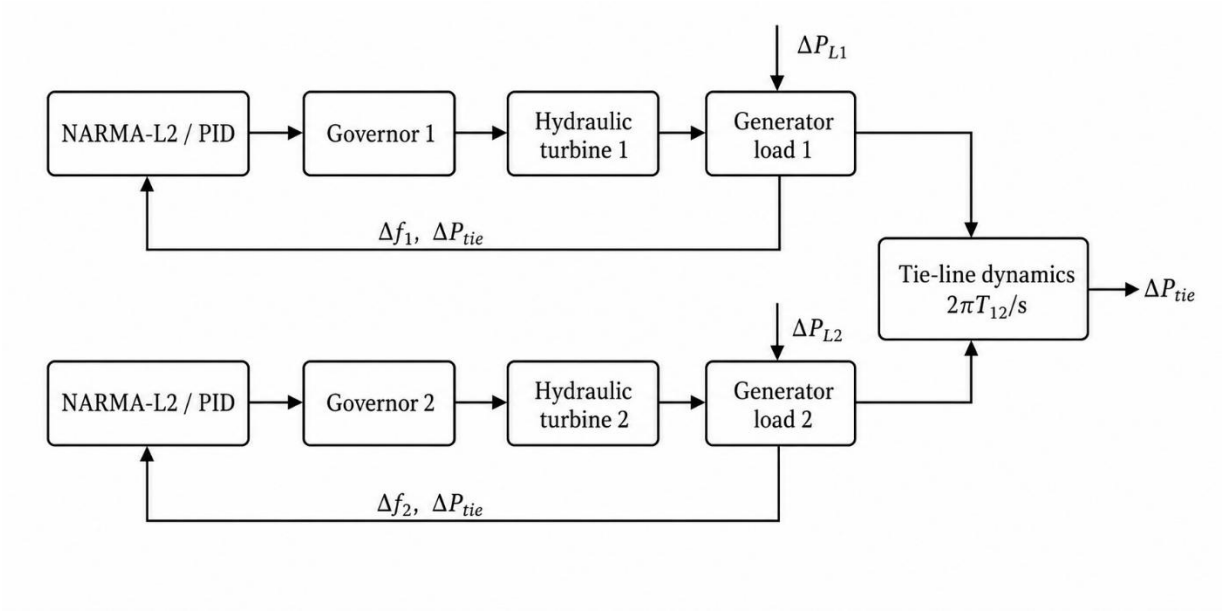

Fig. 1 Two-area hydropower speed-regulation structure.

Table 1. Nominal plant parameters.

Parameter	Area 1	Area 2	Parameter	Value
H_i (s)	5.0	4.5	T_{12} (pu/Hz)	0.0866
D_i (pu/Hz)	1.0	1.1	g_{max} (pu)	0.35
R_i (Hz/pu)	0.05	0.05	$\dot{g}_{max}$ (pu/s)	0.15
R_{ti} (Hz/pu)	0.30	0.32	Sampling time (s)	0.10
T_{gi} (s)	0.20	0.25	Prediction delay d	30 samples
T_{wi} (s)	1.00	1.20	Uncertainty bound	±25%
T_{ri} (s)	5.0	5.5	Simulation time	150 s

IV. CONTROL METHODOLOGIES

A. PID controller

The conventional secondary controller uses $e_i = -ACE_i$ and a filtered derivative:

$$I_i(k) = I_i(k-1) + T_s e_i(k), \quad (10)$$

$$D_i^f(k) = 0.85 D_i^f(k-1) + 0.15 \frac{e_i(k) - e_i(k-1)}{T_s}, \quad (11)$$

$$u_i(k) = K_{pi} e_i(k) + K_{ii} I_i(k) + K_{di} D_i^f(k). \quad (12)$$

The gains are $K_p = 0.05$, $K_i = 0.02$, and $K_d = 0.001$ in both areas. Integral clamping and back-calculation are used when the command reaches the gate limits. These gains provide a stable and well-damped nominal response without excessive actuator movement.

B. Augmented NARMA-L2 neural controller

A general discrete nonlinear plant can be written as a nonlinear autoregressive moving-average model. For a selected relative degree d, the NARMA-L2 approximation rearranges the future output into an input-affine form [18]-[21]:

$$\mathbf{y}(k+d) = \mathbf{F}\big(\mathbf{z}(k)\big) + \mathbf{G}\big(\mathbf{z}(k)\big)\mathbf{u}(k) \quad (13)$$

where $\mathbf{y} = [ACE_1 \ ACE_2]^T$. The augmented regressor is

$$\mathbf{z}(k) = [\mathbf{x}^T(k) \quad \Delta P_{L1}(k) \quad \Delta P_{L2}(k) \quad u_1(k-1) \quad u_2(k-1)]^T. \quad (14)$$

Using estimated governor and turbine states is practical because modern digital governors already measure gate position and contain internal state filters. The load increments may be obtained from local power-balance estimation. The augmentation also avoids requiring a very long output-history vector to reconstruct slow transient-droop states.

Training samples are generated from eight plants whose fifteen main physical parameters are independently varied within ±25%. At each selected state, short forward simulations estimate the affine terms $\mathbf{F}$ and $\mathbf{G}$ by symmetric input perturbation. A single-hidden-layer neural network with 200 hyperbolic-tangent units then maps $\mathbf{z}$ to the six quantities $[F_1, F_2, G_{11}, G_{12}, G_{21}, G_{22}]$. The input and target data are standardized. Hidden weights are deterministic random features, while output weights are obtained by ridge regression:

$$\mathbf{B} = (\mathbf{H}^T\mathbf{H} + \lambda\mathbf{I})^{-1}\mathbf{H}^T\mathbf{Y}, \qquad \lambda = 10^{-4}. \quad (15)$$

The approach is an extreme-learning implementation of the NARMA-L2 approximator. It avoids iterative backpropagation and makes the all-in-one code reproducible without a specialized neural-network toolbox. On the held-out data, the F_1 and F_2 models achieve $R^2 = 0.978$ and $R^2 = 0.974$, respectively. The direct gains are nearly constant for this benchmark, so their low absolute RMSE is more informative than R^2.
At run time, the unconstrained increment is obtained through a damped multivariable inverse:

$$\Delta\mathbf{u}(k) = \left(\widehat{\mathbf{G}}^T\widehat{\mathbf{G}} + \rho\mathbf{I}\right)^{-1}\widehat{\mathbf{G}}^T\left[-\widehat{\mathbf{F}}\right], \qquad \rho = 0.03. \quad (16)$$

The increment is limited to ±0.025 pu per sample and blended with the previous command:

$$\mathbf{u}(k) = \mathrm{sat}_{-0.10}^{0.10}[\mathbf{u}(k-1) + 0.65\Delta\mathbf{u}(k) + 0.002\mathbf{I}_{ACE}(k)]. \quad (17)$$

The regularization in (17) prevents excessive amplification when the estimated gain matrix is poorly conditioned. Figure 2 summarizes the identification and closed-loop procedure, while Fig. 3 shows the held-out regression results.

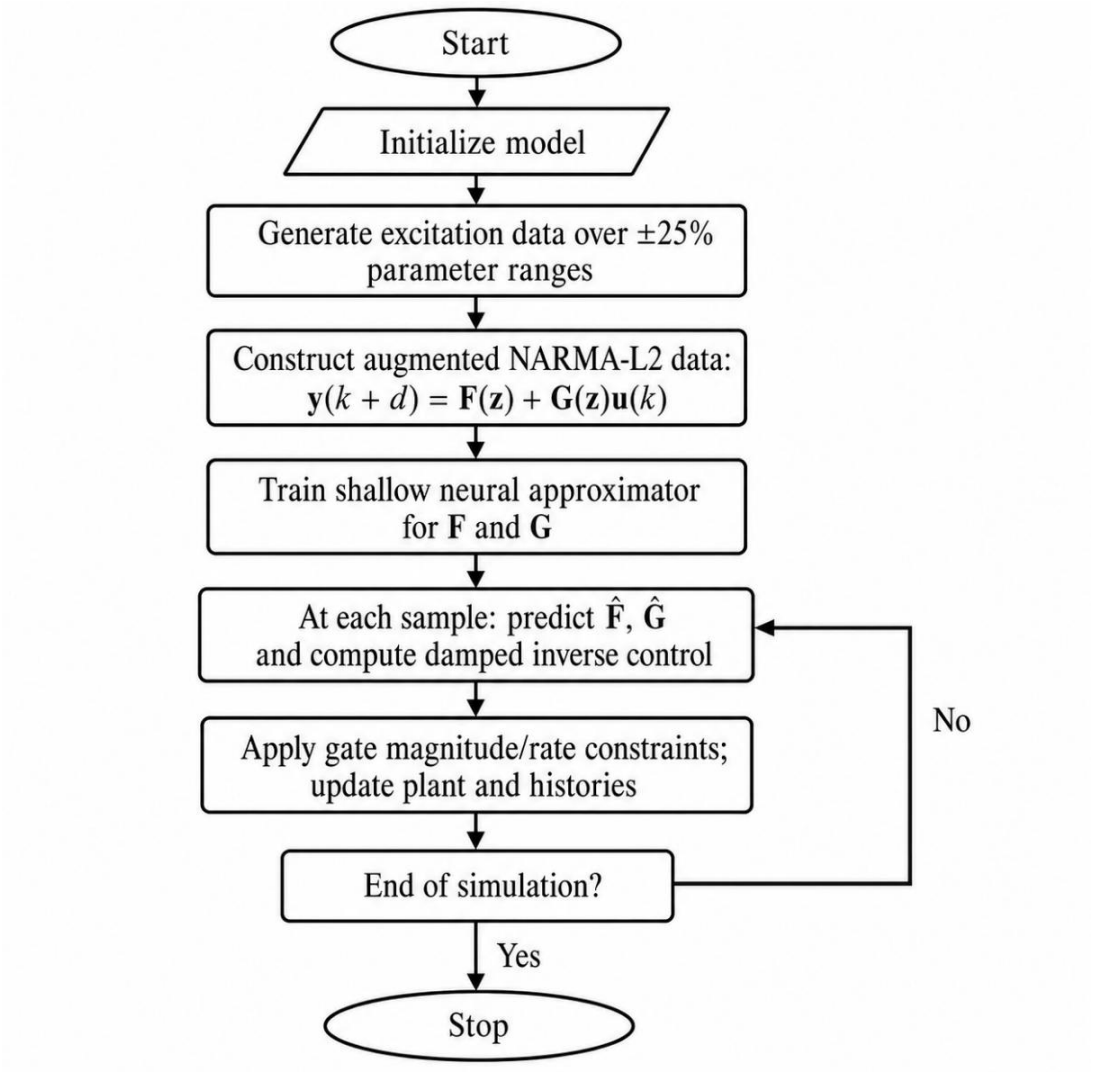

Fig. 2 Identification and online operation of the augmented NARMA-L2 controller.

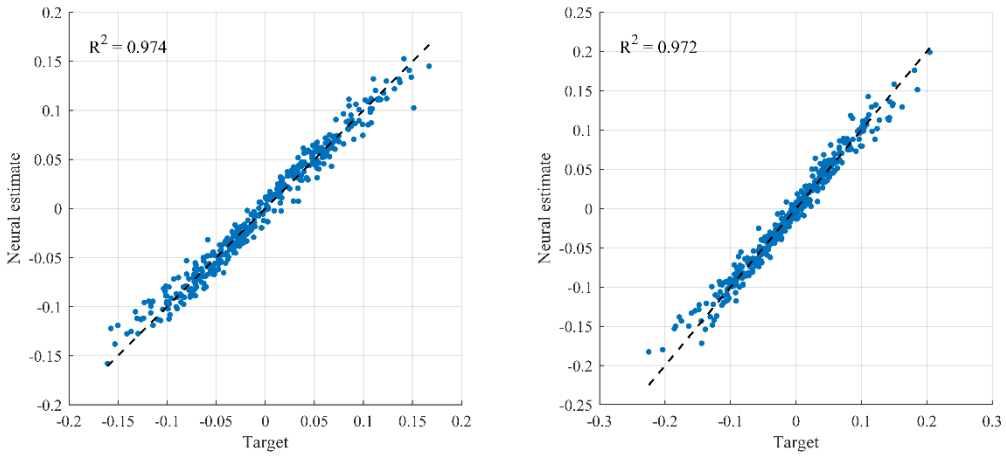

Fig. 3 Held-out regression of the NARMA-L2 affine terms F_1 and F_2.

C. Disturbance and robustness protocol

The step test contains load changes in both areas at 10, 30, 60, 80, 100, and 120 s. It includes positive and negative increments to reveal recovery after successive operating-point changes. The random test combines piecewise-random load levels, first-order smoothing, and low-frequency sinusoidal components. Thus, it is bounded but not periodic and forces the controller to respond continuously.

For the representative uncertain plant, $H_i, D_i, R_i, T_{gi}, T_{wi}, T_{ri}, R_{ti}$, and T_{12} are independently perturbed within ±25%; the PID gains and neural weights remain fixed. A twelve-run Monte-Carlo study repeats the random sampling. This protocol tests robustness to simultaneous parameter changes rather than to isolated one-at-a-time variations.

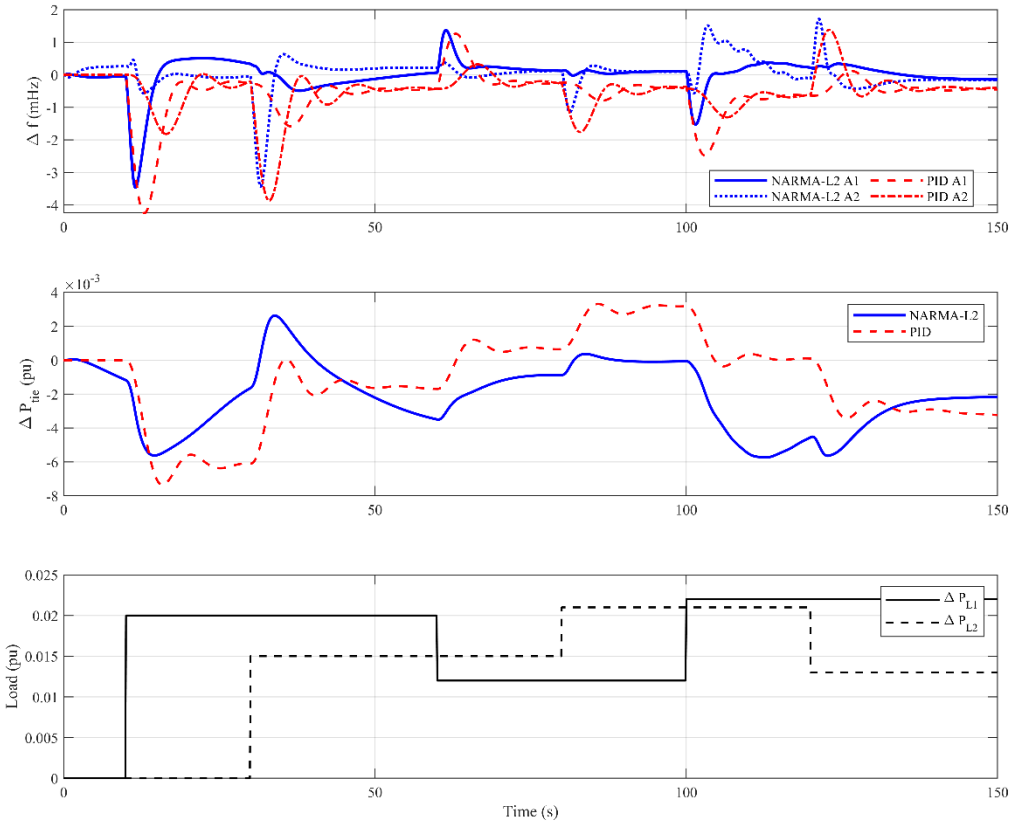

Fig. 4 Nominal-parameter responses under sequential step load changes.

V. SIMULATION AND RESULTS

A. Nominal step-load response

Figure 4 compares the controllers on the nominal plant. The hydraulic inverse response is visible immediately after the first area-1 step: the frequency initially moves away from zero before the governor and water-flow states develop positive mechanical power. NARMA-L2 anticipates the delayed control effect through the 3 s prediction interval. Consequently, the area-1 peak is reduced from 4.251 to 3.480 mHz, and the area-2 peak is reduced from 3.867 to 3.527 mHz. The total frequency IAE decreases by 28.2%, from 0.1799 to 0.1292 Hz·s.

The improvement is not uniform across every quantity. NARMA-L2 produces a peak tie-line deviation of 0.01183 pu, compared with 0.00736 pu for PID. The neural inverse temporarily uses inter-area support more strongly to suppress local speed errors. This behavior is acceptable only when tie-line and actuator constraints are explicitly checked; a frequency-only conclusion would be incomplete.

B. Step loading with parameter variation

The fixed PID controller remains stable under the representative perturbation, but its peak and accumulated errors increase. Area-1 peak deviation rises to 5.002 mHz and total IAE to 0.1924 Hz·s. NARMA-L2 limits the corresponding peak to 4.420 mHz and IAE to 0.1295 Hz·s. The IAE advantage therefore grows from 28.2% in the nominal case to 32.7% under uncertainty.

The neural model was not retrained for the perturbed test. Its robustness arises from two mechanisms: the identification data cover a family of plants, and the damped inverse avoids relying on exact cancellation. The response in Fig. 5 also shows that both controllers remain bounded under gate and gate-rate limits.

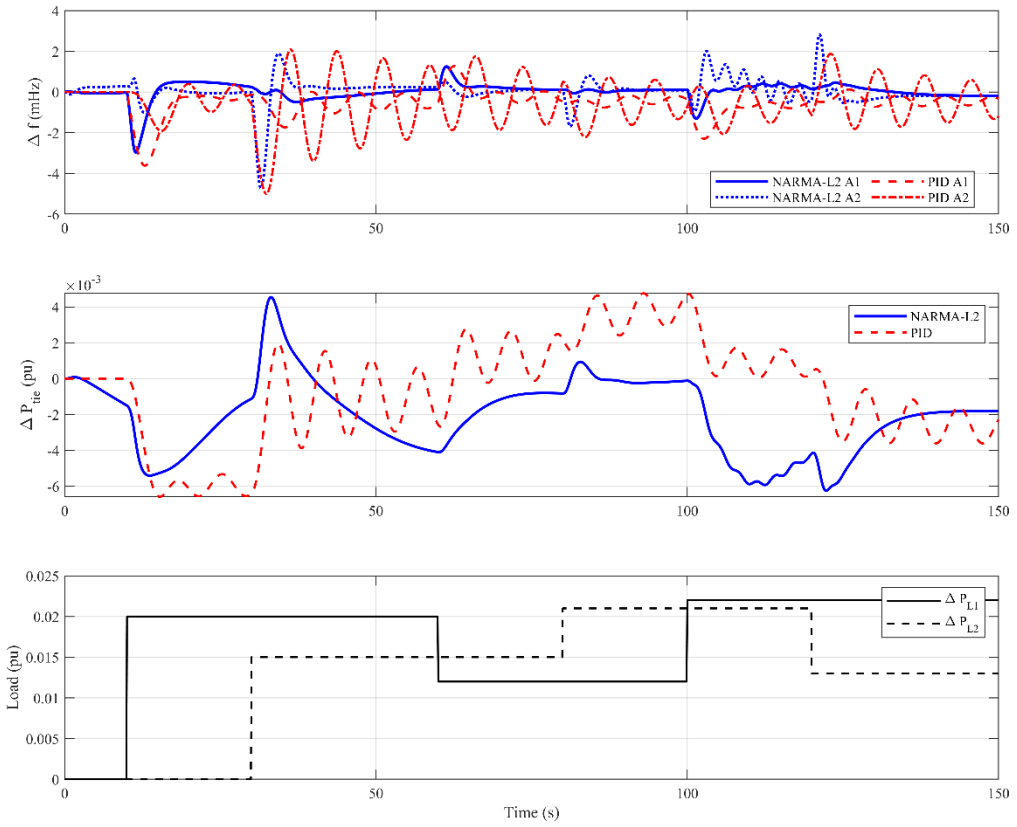

Fig. 5 Responses of the representative ±25% perturbed plant under step load changes.

C. Random load variation

Random loading is more revealing than an isolated step because a controller cannot settle before the next disturbance arrives. Figure 6 shows that PID follows the low-frequency demand changes but retains larger oscillatory components in both areas. NARMA-L2 reduces the maximum deviations from 3.714 and 5.219 mHz to 2.449 and 3.398 mHz. The total IAE is reduced by 41.4%, while the tie-line peak is also lower.

For the perturbed plant in Fig. 7, the area-frequency RMS values with NARMA-L2 are 1.224 and 1.304 mHz. The PID values are 1.997 and 1.785 mHz. Total IAE falls from 0.4591 to 0.3020 Hz·s, a reduction of 34.2%. Unlike the nominal step case, the random-load tie-line excursion is smaller with the neural controller because the multivariable inverse coordinates the two gate commands continuously.

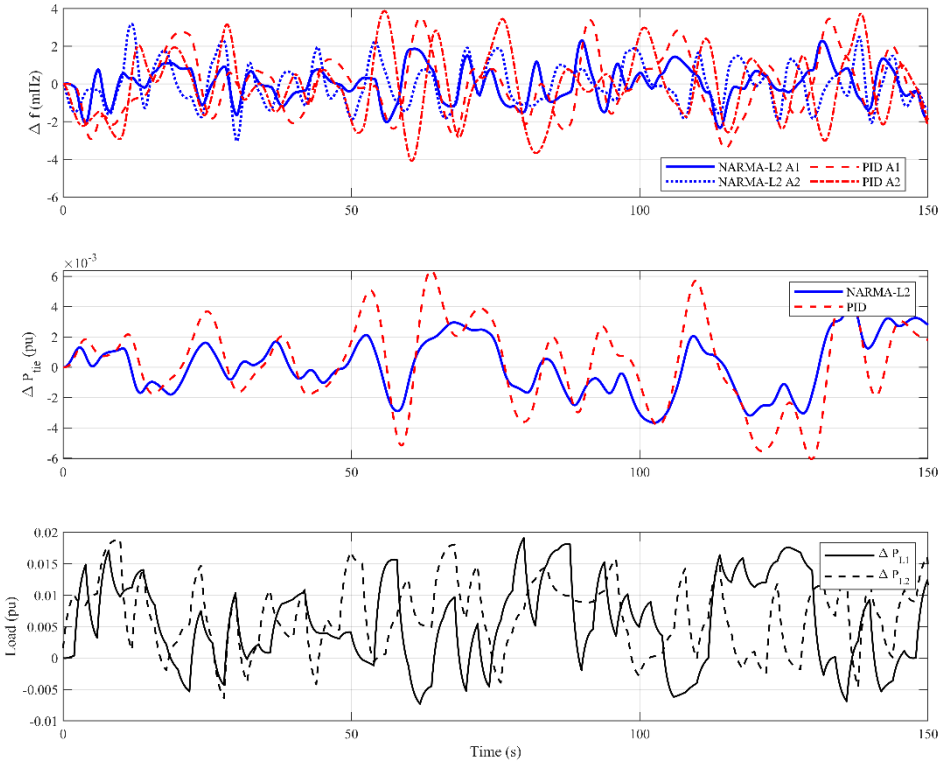

Fig. 6 Nominal-parameter responses under band-limited random load variations.

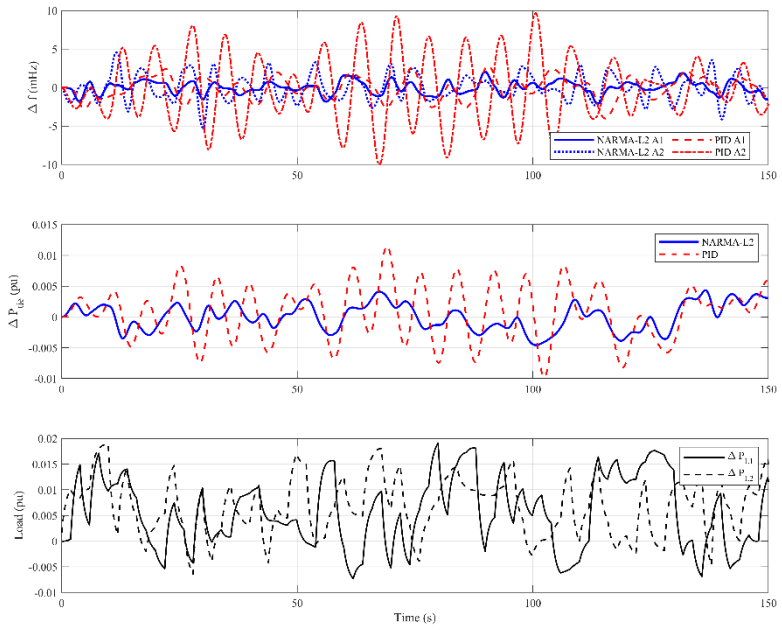

Fig. 7 Responses of the representative ±25% perturbed plant under random load variations.

D. Numerical comparison

Table 2. Principal performance indices for the four test cases.

Scenario	Controller	Peak $\lvert\Delta f_1\rvert$ (mHz)	Peak $\lvert\Delta f_2\rvert$ (mHz)	RMS Δf_1 (mHz)	RMS Δf_2 (mHz)	IAE (Hz·s)	Peak $\lvert\Delta P_{tie}\rvert$ (pu)	RMS control (pu)
Step, nominal	NARMA-L2	3.480	3.527	0.644	0.649	0.1292	0.01183	0.03791
Step, nominal	PID	4.251	3.867	0.908	0.840	0.1799	0.00736	0.01100
Step, uncertain	NARMA-L2	4.420	4.193	0.738	0.676	0.1295	0.01230	0.03835
Step, uncertain	PID	5.002	4.099	1.007	0.909	0.1924	0.00924	0.01104
Random, nominal	NARMA-L2	2.449	3.398	0.931	1.179	0.2543	0.00504	0.03938
Random, nominal	PID	3.714	5.219	1.630	1.844	0.4336	0.00798	0.00781
Random, uncertain	NARMA-L2	3.192	3.817	1.224	1.304	0.3020	0.00683	0.04135
Random, uncertain	PID	4.972	5.308	1.997	1.785	0.4591	0.01015	0.00809

The main cost of the NARMA-L2 improvement is actuator activity. Its RMS command is approximately four to five times the PID value. Figure 8 confirms that the command remains within ±0.10 pu and is smooth at the 0.1 s sampling scale, but the design would require gate-motion and wear constraints before field deployment. The all-in-one code exposes the increment limit, inverse regularization, and command saturation so that this compromise can be retuned.

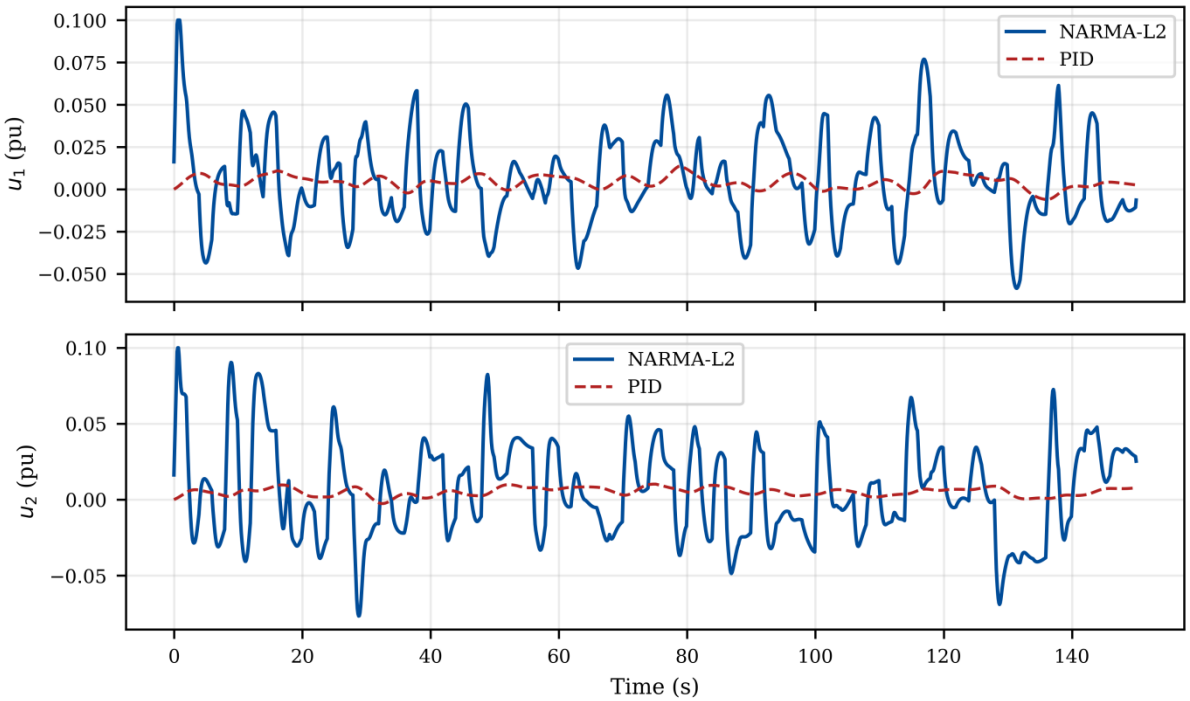

Fig. 8 Control commands for the uncertain plant under random loading.

E. Monte-Carlo robustness

The twelve-run Monte-Carlo study supports the representative-case observations. For step loading, the median total IAE is 0.1019 Hz·s with NARMA-L2 and 0.1543 Hz·s with PID. For random loading, the medians are 0.1809 and 0.2784 Hz·s, respectively. Median aggregate RMS frequency is reduced from 0.942 to 0.655 mHz in the step tests and from 1.468 to 0.964 mHz in the random tests. No unstable realization is observed within the ±25% box.

Figure 9 shows that the IAE distributions remain separated despite simultaneous changes in inertia, damping, droop, governor time constants, water starting times, transient-droop parameters, and tie-line stiffness.

The result does not constitute a formal robust-stability proof, but it provides a stronger empirical assessment than a single nominal step response.

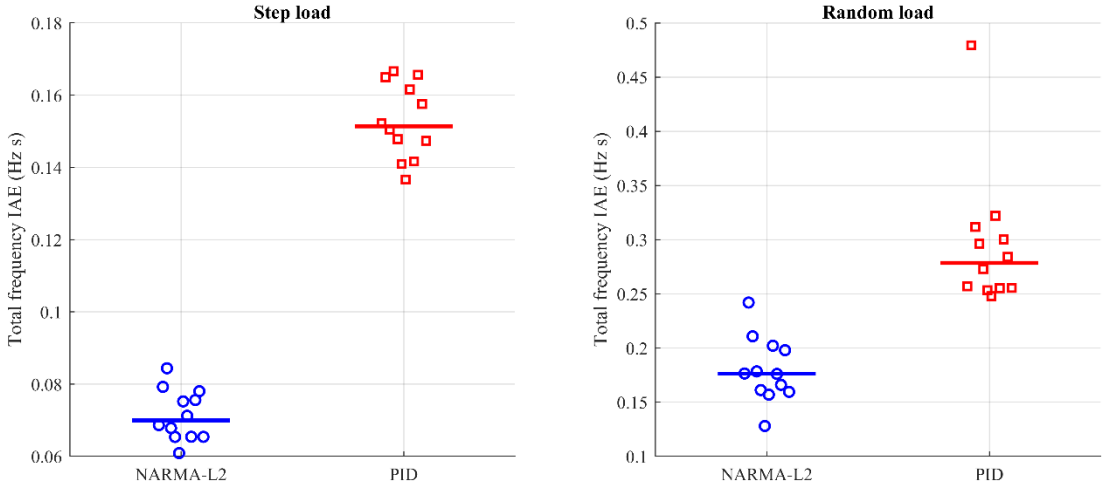

Fig. 9 Monte-Carlo distributions of total frequency IAE for ±25% parameter variation.

The normalized summary in Fig. 10 makes the engineering trade-off explicit. NARMA-L2 improves the average frequency indices and random-load tie-line performance, but its average RMS control action is substantially larger. Thus, the neural method is most suitable when frequency quality has high value and actuator headroom is available. PID is preferable when controller transparency, low gate movement, and minimal commissioning effort are the dominant requirements.

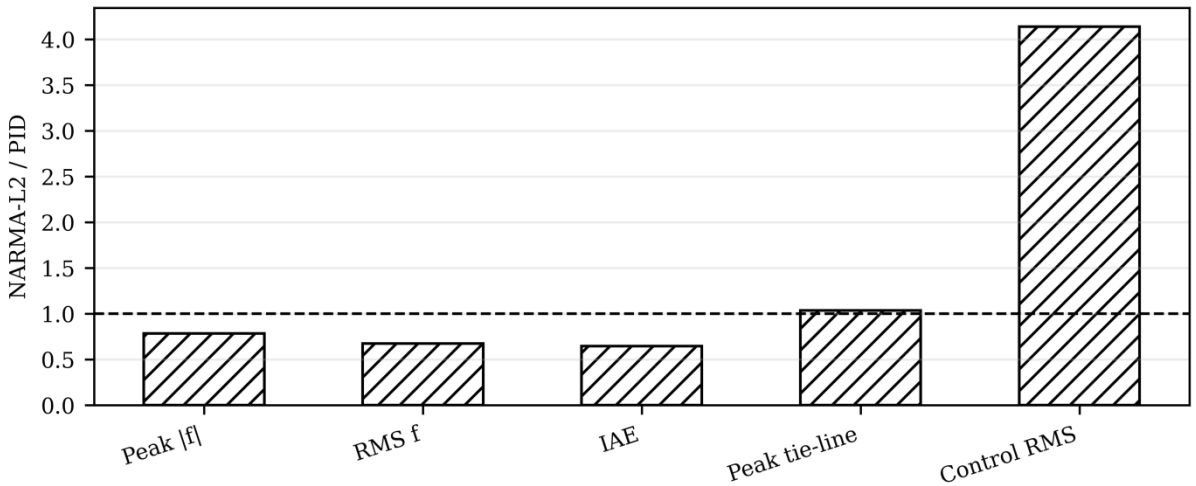

Fig. 10 Scenario-averaged NARMA-L2 metrics normalized by the PID values. Values below one are favorable except for control effort.

VI. CONCLUSION AND FUTURE RESEARCH DIRECTIONS

A reproducible comparison between NARMA-L2 neural control and conventional PID control has been presented for generator-speed regulation in a nonlinear two-area hydropower system. The model includes the hydraulic right-half-plane zero, transient droop, gate magnitude and rate limits, generator-load dynamics, and tie-line coupling. Both controllers remain stable for nominal and ±25% perturbed plants under sequential step and continuously varying random loads.

The NARMA-L2 controller consistently reduces peak and RMS frequency deviations, IAE, and ITAE. Its advantage is most pronounced under random loading, where future-output inversion coordinates the two areas before a conventional fixed-gain loop can fully settle. The robustness study also indicates that identification over a plant family is more effective than training on a single nominal operating point. However, the improvement requires higher gate-command RMS and, for step disturbances, can increase the maximum tie-

line excursion. NARMA-L2 should therefore be implemented with explicit actuator-usage and interchange constraints rather than tuned solely for frequency error.

Future work should validate the controller with nonlinear penstock elasticity, head-dependent turbine efficiency, measurement noise, communication delay, and hardware-in-the-loop governor tests. A constrained neural predictive formulation could further reduce gate wear while preserving the disturbance-rejection benefit observed here.

REFERENCES

[1] H. H. Alhelou, M. E. H. Golshan, R. Zamani, E. Heydarian-Forushani, and P. Siano, "Challenges and opportunities of load frequency control in conventional, modern and future smart power systems: A comprehensive review," *Energies*, vol. 11, no. 10, art. 2497, 2018. doi: 10.3390/en11102497.

[2] S. K. Pandey, S. R. Mohanty, and N. Kishor, "A literature survey on load-frequency control for conventional and distribution generation power systems," *Renewable and Sustainable Energy Reviews*, vol. 25, pp. 318-334, 2013. doi: 10.1016/j.rser.2013.04.029.

[3] K. Ullah, A. Basit, Z. Ullah, S. Aslam, and H. Herodotou, "Automatic generation control strategies in conventional and modern power systems: A comprehensive overview," *Energies*, vol. 14, no. 9, art. 2376, 2021. doi: 10.3390/en14092376.

[4] M. Ranjan and R. Shankar, "A literature survey on load frequency control considering renewable energy integration in power system: Recent trends and future prospects," *Journal of Energy Storage*, vol. 45, art. 103717, 2022. doi: 10.1016/j.est.2021.103717.

[5] I. A. Khan, H. Mokhlis, N. N. Mansor, H. A. Illias, L. J. Awalin, and L. Wang, "New trends and future directions in load frequency control and flexible power system: A comprehensive review," *Alexandria Engineering Journal*, pp. 263-308, 2023. doi: 10.1016/j.aej.2023.03.040.

[6] W. Guo and J. Yang, "Modeling and dynamic response control for primary frequency regulation of hydro-turbine governing system with surge tank," *Renewable Energy*, vol. 121, pp. 173-187, 2018. doi: 10.1016/j.renene.2018.01.022.

[7] T. Reigstad and K. Uhlen, "Variable-speed hydropower generation: System modeling, optimal control, and experimental validation," *IEEE Transactions on Industrial Electronics*, vol. 68, no. 11, pp. 10902-10912, 2021. doi: 10.1109/TIE.2020.3031528.

[8] U.S. Department of Energy, "Hydropower Modeling Gaps in Planning and Operational Studies," 2022. URL: https://www.energy.gov/sites/default/files/2023-07/Hydropower_Modeling_Gaps.pdf.

[9] L. Saarinen, "On Hydropower and Grid Frequency Control," KTH Royal Institute of Technology, 2017. URL: https://www.diva-portal.org/smash/get/diva2:1050397/FULLTEXT01.pdf.

[10] M. Masmali, "Comparative studies on load frequency control with hydropower governor models," *Engineering, Technology & Applied Science Research*, vol. 14, 2024. URL: https://etasr.com/index.php/ETASR/article/download/6722/3464/25229.

[11] V. P. Singh, N. Kishor, and P. Samuel, "Improved load frequency control of power system using LMI based PID approach," *Journal of the Franklin Institute*, vol. 354, pp. 6805-6830, 2017. doi: 10.1016/j.jfranklin.2017.08.031.

[12] Y. Arya, "Automatic generation control of two-area electrical power systems via optimal fuzzy classical controller," *Journal of the Franklin Institute*, vol. 355, pp. 2662-2688, 2018. doi: 10.1016/j.jfranklin.2018.02.004.

[13] N. Jalali, H. Razmi, and H. Doagou-Mojarrad, "Optimized fuzzy self-tuning PID controller design based on Tribe-DE optimization and rule-weight adjustment for load frequency control of interconnected multi-area power systems," *Applied Soft Computing*, art. 106424, 2020. doi: 10.1016/j.asoc.2020.106424.

[14] D. K. Gupta *et al.*, "Load frequency control using hybrid intelligent optimization technique for multi-source power systems," *Energies*, vol. 14, no. 6, art. 1581, 2021. doi: 10.3390/en14061581.

[15] A. M. A. Soliman *et al.*, "PSO tuned interval type-2 fuzzy logic for load frequency control of two-area multi-source interconnected power system," *Scientific Reports*, vol. 13, art. 8724, 2023. doi: 10.1038/s41598-023-35454-4.

[16] J. Sharma *et al.*, "Robust PID load frequency controller design with specific gain and phase margin for multi-area power systems," *IFAC-PapersOnLine*, pp. 627-632, 2018. doi: 10.1016/j.ifacol.2018.06.166.

[17] V. Çelik, "Effects of fractional-order PI controller on delay margin in single-area delayed load frequency control systems," *Journal of Modern Power Systems and Clean Energy*, vol. 7, pp. 380-389, 2019. doi: 10.1007/s40565-018-0458-5.

[18] P. Sharma, "NARMA-L2 controller for five-area load frequency control," *Indonesian Journal of Electrical Engineering and Informatics*, vol. 2, no. 4, pp. 170-179, 2014. doi: 10.11591/ijeei.v2i4.123.

[19] D. K. Sambariya and V. Nath, "Application of NARMA L2 controller for load frequency control of multi-area power system," in *2016 10th International Conference on Intelligent Systems and Control*, pp. 1-7, 2016. doi: 10.1109/ISCO.2016.7726987.

[20] MathWorks, "Design NARMA-L2 Neural Controller in Simulink," Deep Learning Toolbox Documentation, 2026. URL: https://www.mathworks.com/help/deeplearning/ug/design-narma-l2-neural-controller-in-simulink.html.

[21] A. Gundogdu and R. Celikel, "NARMA-L2 controller for stepper motor used in single-link manipulator with low-speed-resonance damping," *Engineering Science and Technology, an International Journal*, vol. 24, no. 2, pp. 360-371, 2021. doi: 10.1016/j.jestch.2020.09.008.

[22] R. Dash *et al.*, "An approach for load frequency control enhancement in two-area hydro-wind power systems using LSTM + GA-PID controller with augmented Lagrangian methods," *Scientific Reports*, vol. 15, art. 1307, 2025. doi: 10.1038/s41598-025-85639-2.

[23] C. K. Shiva, V. Mukherjee, and S. P. Ghoshal, "Automatic generation control of hydropower systems using a novel quasi-oppositional harmony search algorithm," *Electric Power Components and Systems*, pp. 1478-1491, 2016. doi: 10.1080/15325008.2016.1147103.

[24] R. Patel *et al.*, "Enhancing optimal automatic generation control in a multi-area power system with diverse energy resources," *IEEE Transactions on Power Systems*, vol. 34, pp. 3465-3475, 2019. doi: 10.1109/TPWRS.2019.2907614.

[25] J. Guo, "Application of full order sliding mode control based on different areas power system with load frequency control," *ISA Transactions*, pp. 23-34, 2019. doi: 10.1016/j.isatra.2019.01.036.

[26] J. Guo, "Application of a novel adaptive sliding mode control method to the load frequency control," *European Journal of Control*, pp. 172-178, 2021. doi: 10.1016/j.ejcon.2020.03.007.

[27] S. Prasad, S. Purwar, and N. Kishor, "Non-linear sliding mode load frequency control in multi-area power system," *Control Engineering Practice*, vol. 61, pp. 81-92, 2017. doi: 10.1016/j.conengprac.2017.02.001.

[28] S. Prasad, S. Purwar, and N. Kishor, "Load frequency regulation using observer-based nonlinear sliding mode control," *International Journal of Electrical Power & Energy Systems*, pp. 178-193, 2019. doi: 10.1016/j.ijepes.2018.06.035.

[29] D. Qian, "Load frequency control by neural-network-based integral sliding mode for nonlinear power systems with wind turbines," *Neurocomputing*, pp. 875-885, 2016. doi: 10.1016/j.neucom.2015.08.043.

[30] A. Sharma *et al.*, "Integrating layered recurrent ANN with robust control strategy for diverse operating conditions of AGC of the power system," *IET Generation, Transmission & Distribution*, 2020. doi: 10.1049/iet-gtd.2019.0935.

[31] X. Su *et al.*, "Event-triggered sliding-mode control for multi-area power systems," *IEEE Transactions on Industrial Electronics*, vol. 64, pp. 6732-6741, 2017. doi: 10.1109/TIE.2017.2677357.
[32] W. Shangguan *et al.*, "Control-performance-standards-oriented event-triggered load frequency control for power systems under limited communication bandwidth," *IEEE Transactions on Control Systems Technology*, pp. 860-868, 2022. doi: 10.1109/TCST.2021.3070861.
[33] R. K. Sahu, S. Panda, and U. K. Rout, "Automatic generation control of multi-area power systems with diverse energy sources using teaching-learning-based optimization algorithm," *Engineering Science and Technology, an International Journal*, vol. 19, pp. 113-134, 2016. doi: 10.1016/j.jestch.2015.07.011.
[34] R. K. Sahu, S. Panda, and G. T. C. Sekhar, "A hybrid DE-PS algorithm for load frequency control under deregulated power system with UPFC and RFB," *Ain Shams Engineering Journal*, vol. 6, pp. 893-911, 2015. doi: 10.1016/j.asej.2015.03.011.
[35] R. Shankar, "Small-signal stability analysis for two-area interconnected power system with load frequency controller in coordination with FACTS and energy storage device," *Ain Shams Engineering Journal*, vol. 7, pp. 603-612, 2016. doi: 10.1016/j.asej.2015.06.009.
[36] N. Hakimuddin *et al.*, "Optimal automatic generation control with hydro, thermal, gas, and wind power plants in a two-area interconnected power system," *Electric Power Components and Systems*, pp. 558-571, 2020. doi: 10.1080/15325008.2020.1793829.
[37] V. V. Huynh *et al.*, "Load frequency control for multi-area power plants with integrated wind resources," *Applied Sciences*, vol. 11, no. 7, art. 3051, 2021. doi: 10.3390/app11073051.
[38] V. V. Huynh *et al.*, "Highly robust observer sliding-mode-based frequency control for multi-area power systems with renewable power plants," *Electronics*, vol. 10, no. 3, art. 274, 2021. doi: 10.3390/electronics10030274.
[39] M. K. Sarkar and A. Dev, "Chattering-free robust adaptive integral higher-order sliding mode control for load frequency problems in multi-area power systems," *IET Control Theory & Applications*, pp. 1216-1227, 2018. doi: 10.1049/iet-cta.2017.0735.
[40] H. Bevrani, *Robust Power System Frequency Control*, 2nd ed. Springer, 2014. doi: 10.1007/978-3-319-07278-4.